How to cite: *Angew. Chem. Int. Ed.* **2021**, *60*, 15632–15640
International Edition: doi.org/10.1002/anie.202104916
German Edition: doi.org/10.1002/ange.202104916

O_2 Activation Hot Paper

Dioxygen Activation and Pyrrole α-Cleavage with Calix[4]pyrrolato Aluminates: Enzyme Model by Structural Constraint

*Lukas Maximilian Sigmund, Christopher Ehlert, Markus Enders, Jürgen Graf, Ganna Gryn'ova, and Lutz Greb**

Abstract: *The present work describes the reaction of triplet dioxygen with the porphyrinogenic calix[4]pyrrolato aluminates to alkylperoxido aluminates in high selectivity. Multiconfigurational quantum chemical computations disclose the mechanism for this spin-forbidden process. Despite a negligible spin–orbit coupling constant, the intersystem crossing (ISC) is facilitated by singlet and triplet state degeneracy and spin–vibronic coupling. The formed peroxides are stable toward external substrates but undergo an unprecedented oxidative pyrrole α-cleavage by ligand aromatization/dearomatization-initiated O–O σ-bond scission. A detailed comparison of the calix[4]pyrrolato aluminates with dioxygen-related enzymology provides insights into the ISC of metal- or cofactor-free enzymes. It substantiates the importance of structural constraint and element–ligand cooperativity for the functions of aerobic life.*

Introduction

Literally vital to all processes of aerobic life is the selective activation of dioxygen and the control over deleterious intermediates.[1] The spin barrier that kinetically protects singlet molecules from spontaneous combustion with triplet dioxygen is bypassed, e.g., with flavin cofactors in flavoenzymes (Figure 1 A),[2] with iron centers as in intra- or extradiol dioxygenases (Figure 1 B),[3] or with iron porphyrins in heme proteins (Figure 1 C).[4] In flavoenzymes, O_2 is reduced by the organic electron donor flavin and bound as hydroperoxide.[2,5] Iron porphyrins capture O_2 as ferric superoxide upon oxidation of Fe^{II}, whereas in intra-/extradiol dioxygenases, O_2 binding occurs cooperatively between the metal and a catechol-type substrate.[3,4] A common black box in all these processes is the critical intersystem crossing (ISC). In some cases, a proton-coupled electron transfer (PCET) enables a mild one-electron reduction of dioxygen.[5,6] For iron-containing enzymes, the ISC is proposed to rely on the spin-mediating role of the open d-shell, but for closed-shell cofactors, the ISC is less well elucidated.[7,8] When it comes to the downstream chemistry of dioxygen-activated intermediates, a huge variety of possibilities arises.[9] Because most oxygen-bound intermediates have a short lifetime and are challenging to characterize, mechanistic elucidations of these processes required combined computational, spectroscopic, and crystallographic efforts or profit from molecular model systems.[10]

The reduced congeners of the porphyrins are the calix[4]pyrroles (porphyrinogens), having $C(sp^3)$-linked pyrroles without π-conjugation among the heterocyclic units (see Figure 1 D for a calix[4]pyrrole aluminum complex).[11] The synthetic connection between calix[4]pyrroles and porphyrins by stepwise oxidation and group transfer from the *meso*-positions has been thoroughly studied by Floriani, Scott, and Nocera.[12] Thus, the calix[4]pyrroles offer ligand-based, multi-electron redox-chemistry that is not amenable to the native heme cofactors. Still, their involvement in dioxygen binding has not been investigated yet. We previously employed the calix[4]pyrrolates as ligands to force aluminum into a unique, square-planar coordination environment with unusual Lewis acidity (Figure 1 D).[13] Due to the electron-rich pyrrole rings in close vicinity to the Al^{III} center, the calix[4]pyrrolato aluminates show ambiphilic reactivity toward polarized substrates by aluminum–ligand cooperativity (AlLC).[14] Whereas metal–ligand cooperative (MLC) binding of O_2 has been well studied with complexes of transition metals,[10e,15–19] the element–ligand cooperative (ELC) reaction of O_2 with p-block compounds is limited to antimony(V).[20] A substantial number of p-block-based species react with molecular oxygen in different modes, but in all cases, the thermodynamic and kinetic feasibility is provided by low-valency or strongly reducing metal–alkyl bonds.[21] Herein, we describe how the selective activation and transformation of dioxygen with a p-block element is enabled in its common

[*] L. M. Sigmund, Prof. Dr. M. Enders, Priv.-Doz. Dr. L. Greb
Anorganisch-Chemisches Institut
Ruprecht-Karls-Universität Heidelberg
Im Neuenheimer Feld 270, 69120 Heidelberg (Germany)
E-mail: greb@uni-heidelberg.de
Dr. C. Ehlert, Dr. G. Gryn'ova
Heidelberg Institute for Theoretical Studies (HITS gGmbH)
Schloss-Wolfsbrunnenweg 35, 69118 Heidelberg (Germany),
and
Interdisciplinary Center for Scientific Computing (IWR)
Ruprecht-Karls-Universität Heidelberg
Im Neuenheimer Feld 205, 69120 Heidelberg (Germany)
Dr. J. Graf
Organisch-Chemisches Institut
Ruprecht-Karls-Universität Heidelberg
Im Neuenheimer Feld 270, 69120 Heidelberg (Germany)
Supporting information and the ORCID identification number(s) for the author(s) of this article can be found under: https://doi.org/10.1002/anie.202104916.

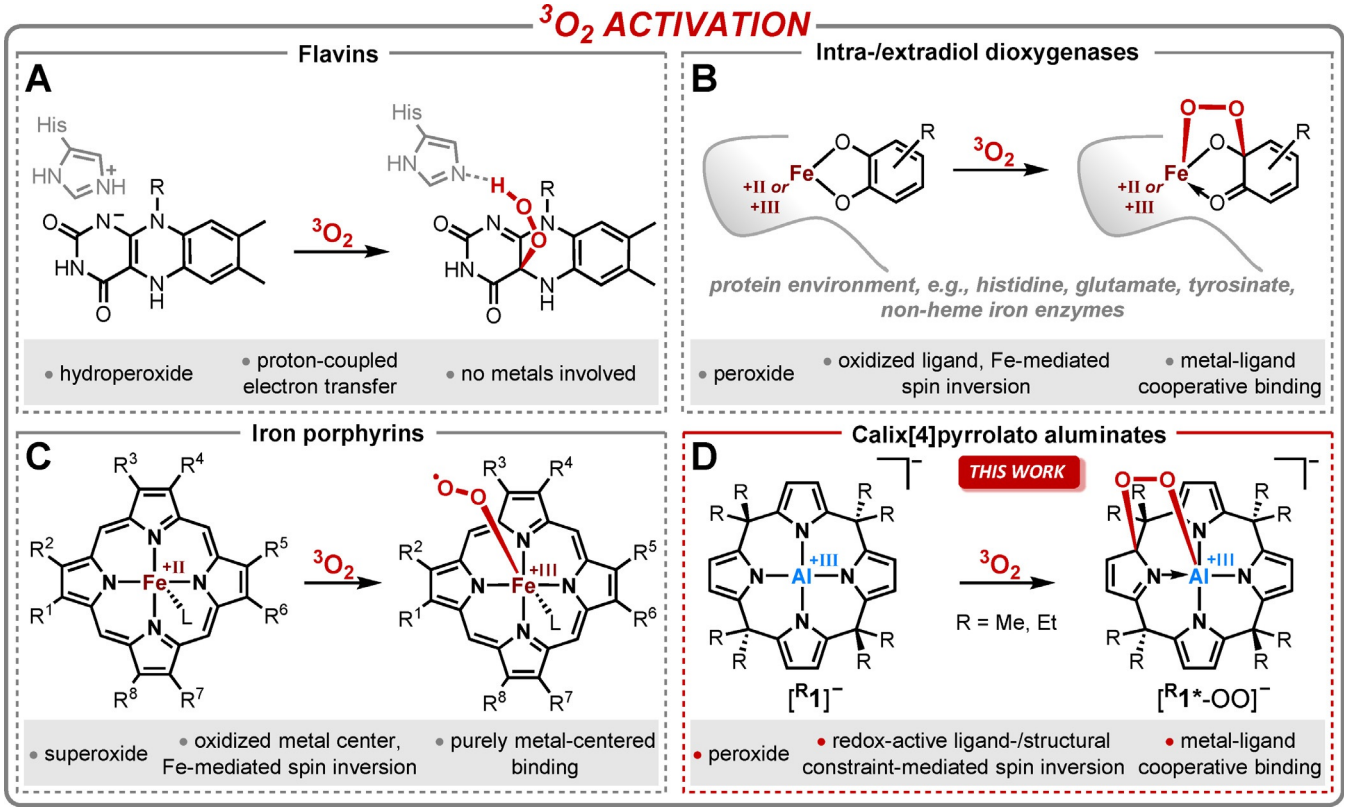

Figure 1. Reactivity of A) flavins in flavoenzymes, B) intra-/extradiol dioxygenases, C) iron porphyrins in heme proteins, with triplet dioxygen, and D) its reactivity with calix[4]pyrrolato aluminates described in this work. The asterisk in $[^R1$*-OO$]^-$ stands for one dearomatized pyrrole ring within the calix[4]pyrrolato ligand.

oxidation state by the effect of structural constraint and element–ligand cooperativity.

We report on the spontaneous reaction of the *meso*-octaalkylcalix[4]pyrrolato aluminates ($[^R1]^-$, R = Me, Et) with dioxygen (Figure 1 D). The dioxygen activation proceeds in analogy to the PCET-mediated sense of metal- and porphyrin-free flavoenzymes,[5] and the subsequent oxidative ring cleavage can be compared with extra- or intradiol dioxygenases.[3,10] Hence, the calix[4]pyrrolato aluminate serves as a straightforward enzyme model highlighting the importance of structural constraint and element–ligand cooperativity for chemistry and biology.

Results and Discussion

When $[PPh_4][^{Me}1]$ or $[PPh_4][^{Et}1]$ in [D$_2$]dichloromethane was subjected to 1 bar of dioxygen gas at room temperature, the appearance of the reaction solution changed from colorless to orange within seconds (Figure 2 A). The ^{1}H NMR spectrum revealed complete consumption of the starting material and the formation of a new C_1-symmetric species (Figure 2 B). This pattern indicates one dearomatized pyrrole ring as it was already observed for $[^{Me/Et}1]^-$ upon interaction with carbonylic[14b] and protic[14c] substrates. We thus assumed an aluminum–ligand cooperative binding of O_2 to $[^{Me/Et}1]^-$ by the formation of an alkylperoxido aluminate, $[^{Me}1$*-OO$]^-$ and $[^{Et}1$*-OO$]^-$, respectively (Figure 2 A, the asterisk indicates the dearomatization of one pyrrole unit within the calix[4]pyrrolato ligand).

SCXRD analysis with single crystals of $[PPh_4][^{Me}1$*-OO] unequivocally confirmed this assumption (Figure 2 C). In $[^{Me}1$*-OO$]^-$, the dearomatized state of one pyrrole ring becomes apparent from the average bond angle of 109.3(1)° around the now sp^3-hybridized carbon atom connected to the peroxido group. The C–N and C–C bond lengths within this ring support this picture. The alkylperoxido moiety features a C(sp^3)–O distance of 143.11(19) pm and is bound to the aluminum center via an Al–O bond of 183.11(12) pm in length. The latter is slightly shorter than the Al–O bond in $[^{Me}1$*-CO$_2]^-$ (184.8(3) pm),[14b] but longer than aluminum oxygen distances in other aluminum alkylperoxides (172–176 pm).[21c,h,j,22] The interoxygen distance experiences a significant elongation from 120.8 pm for $^3O_2$ in the gas phase[23] to 148.79(14) pm in $[^{Me}1$*-OO$]^-$, consistent with the two-electron reduction of O_2 to the peroxidic oxidation state. Similar distances (146–149 pm) are found for other alkylperoxido complexes from transition metal–ligand cooperative binding of dioxygen.[10e,16,19b,20a] Intriguingly, the capture of O_2 with $[PPh_4][^{Me}1]$ occurred equally, though less efficient, simply under air instead of pure dioxygen gas. The reaction also takes place in the absence of light. The binding of O_2 to both aluminates was found irreversible and could not be reversed under reduced pressure or elevated temperature. Notably, the reaction of dioxygen with a dianionic Co^{II} complex of the same ligand did not result in the

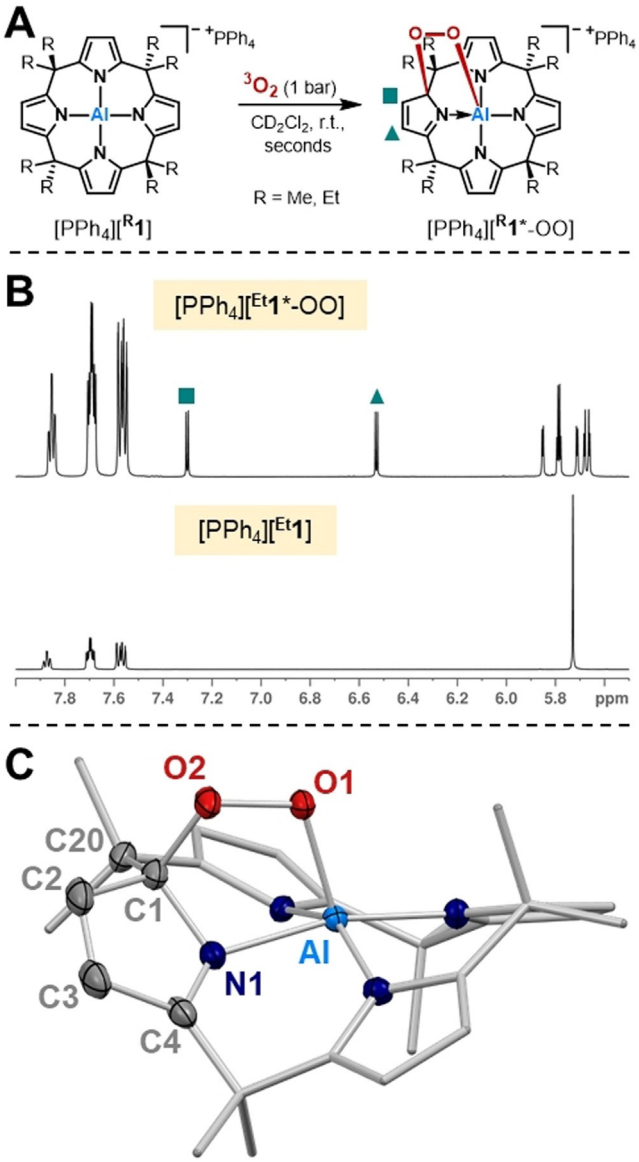

Figure 2. A) Reaction scheme for dioxygen with $[PPh_4][^{Me/Et}\mathbf{1}]$. The asterisk in $[^{Me}\mathbf{1}^*\text{-OO}]$ indicates the dearomatization of one pyrrole unit within the calix[4]pyrrolato ligand. B) Tetraphenylphosphonium/pyrrole section of the ^{1}H NMR spectrum (600 MHz, CD_2Cl_2) of $[PPh_4][^{Et}\mathbf{1}]$ and $[PPh_4][^{Et}\mathbf{1}^*\text{-OO}]$. C) Molecular structure of $[^{Me}\mathbf{1}^*\text{-OO}]^-$ as determined by SCXRD analysis.[38] Thermal displacement ellipsoids are shown at a probability of 50%. The PPh_4^+ cation, cocrystallized dichloromethane, and all hydrogen atoms are omitted. Selected bond lengths [pm]: Al–O1: 183.11(12), O1–O2: 148.79(14), O2–C1: 143.11(19), C1–C2: 151.9(2), C2–C3: 132.9(3), C3–C4: 148.1(2), C4–N1: 128.3(2). Selected bond angles [°]: N1-C1-C2: 102.63(13), C20-C1-C2: 115.81(14), N1-C1-C20: 110.33(13), O2-C1-N1: 105.18(12), O2-C1-C2: 106.32(13), O2-C1-C20: 115.33(13), C1-O2-O1: 109.77(10), O2-O1-Al: 112.33(8).

formation of an alkylperoxide but induced the two-electron oxidation of the ligand framework.[24] On the other hand, aluminum pyrrolato complexes with aluminum–alkyl groups engaged via the common insertion of O_2 into the carbon–aluminum bond.[21o]

To understand the mechanism of this unusual addition of triplet O_2 to the singlet-state aluminates, quantum chemical calculations were carried out for $[^{Me}\mathbf{1}]^-$. At first, the course of the reaction was evaluated by density functional theory (DFT) on the B97M-D3(BJ)/def2-TZVPP, COSMO-RS-(CH_2Cl_2) level (Figure 3A). Given the redox potential of the O_2/O_2^- couple (−1.3 V vs. Fc in acetonitrile)[25] in comparison to the electron donor capability of $[^{Me}\mathbf{1}]^-$ (+0.1 V onset potential for the first oxidation wave in the cyclic voltammogram of $[PPh_4][^{Me}\mathbf{1}]$ in CH_2Cl_2, see Figure S5 in the Supporting Information), an outer-sphere electron transfer was ruled out as the initial step. Instead, dioxygen approaches $[^{Me}\mathbf{1}]^-$ through a first transition state (**TS-1A**), which is located on the triplet potential energy surface with a Gibbs free energy barrier of 59.3 kJ mol^{-1} (Figure 3A). In **TS-1A**, the coordinating oxygen atom is separated from the aluminum center by 237 pm, and the O–O distance amounts to 123 pm. The natural spin density is predominantly located on the dioxygen unit (90%). The energies of the closed-shell (CSS) and open-shell singlet (OSS) state (broken symmetry approach) are significantly higher in energy (80.6 kJ mol^{-1} for ^{CSS}**TS-1A** and 56.8 kJ mol^{-1} for ^{OSS}**TS-1A**, relative to ^{triplet}**TS-1A**), ruling out a spin state change happening before the association. The triplet state preference in **TS-1A** is rooted in the ferromagnetic spin coupling of the two unpaired electrons still mainly residing in the pseudo-orthogonal π*-orbitals at dioxygen.[26] The subsequent local minimum structure ($^3[^{Me}\mathbf{1}\text{-}O_2]^-$) is essentially Gibbs isoenergetic to the starting materials and enthalpically favored by 43.5 kJ mol^{-1}. This unusually strong interaction of an anionic Lewis acid with the weak Lewis base O_2 is the consequence of 1) the structural constraint-induced Lewis acidity of $[^{Me}\mathbf{1}]^-$,[13] and 2) the redox-noninnocence of the ligand, as explained in the next paragraph.

Compared to **TS-1A**, the Al–O distance in $^3[^{Me}\mathbf{1}\text{-}O_2]^-$ decreases to 184 pm while the O–O bond length increases to 134 pm. Hence, the O_2 moiety is reduced to the superoxide redox-state, whereas the calix[4]pyrrolato ligand gets oxidized by one electron. This picture is supported by the natural spin density within $^3[^{Me}\mathbf{1}\text{-}O_2]^-$, which is now equally distributed between the dioxygen and the ligand backbone (Figure 3A). The natural charge of the O_2 fragment changes from 0.07 in **TS-1A** to −0.75 in $^3[^{Me}\mathbf{1}\text{-}O_2]^-$. The final alkylperoxido aluminate $[^{Me}\mathbf{1}^*\text{-OO}]^-$ is formed after the transition to the singlet potential energy surface and C–O bond formation (see next paragraph). The overall reaction is found exergonic by −79.0 kJ mol^{-1} ($\Delta_R H = -134.7$ kJ mol^{-1}).

For a description of the spin-forbidden conversion from $^3[^{Me}\mathbf{1}\text{-}O_2]^-$ to $[^{Me}\mathbf{1}^*\text{-OO}]^-$, structure optimizations for singlet and triplet states using a multireference approach based on the complete active space self-consistent field method (CASSCF) were performed (for details, see Chapter S7 of the Supporting Information). In accordance with the DFT calculations, a triplet minimum was obtained for the end-on association structure ($^3[^{Me}\mathbf{1}\text{-}O_2]^-$). However, a multireference open-shell singlet minimum ($^1[^{Me}\mathbf{1}\text{-}O_2]^-$) was also identified with a nearly identical structure (RMSD = 0.67 pm) and energy ($\Delta E^{singlet/triplet} = 0.09$ kJ mol^{-1} at the CASSCF/def2-SVP level of theory). Starting from $^1[^{Me}\mathbf{1}\text{-}O_2]^-$, a constrained CASSCF potential energy surface scan toward the structure of the final closed-shell singlet $[^{Me}\mathbf{1}^*\text{-OO}]^-$ was conducted

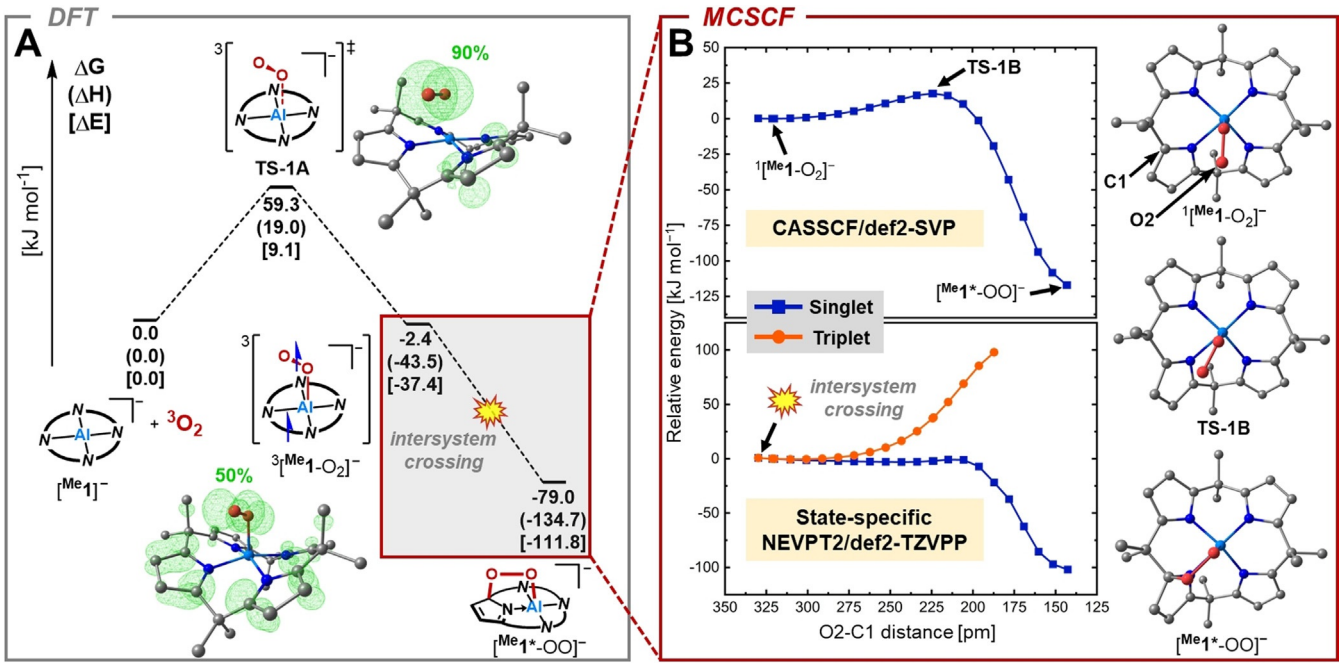

Figure 3. A) Energy profile for the addition reaction of $^3O_2$ to $[^{Me}\mathbf{1}]^-$ computed with DFT at the B97M-D3(BJ)/def2-TZVPP level. Gibbs free energies and enthalpies include COSMO-RS(CH_2Cl_2) solvation correction. The depicted natural spin density distributions were calculated with PBE0/def2-TZVPP. B) Singlet CASSCF(14,13)/def2-SVP constrained potential energy surface scan between $^1[^{Me}\mathbf{1}\text{-}O_2]^-$ and $[^{Me}\mathbf{1}^*\text{-}OO]^-$ and state-specific NEVPT2(14,13)/def2-TZVPP triplet and singlet energies for each constrained minimum structure.

(Figure 3B, upper panel). A minimum structure similar to DFT was obtained for $[^{Me}\mathbf{1}^*\text{-}OO]^-$. Notably, a proper transition state corresponding to the formation of the C–O bond was identified in between $^1[^{Me}\mathbf{1}\text{-}O_2]^-$ and $[^{Me}\mathbf{1}^*\text{-}OO]^-$ (**TS-1B**, C–O distance: 224 pm) that would not be accessible by single-reference methods. The energetic barrier of 17.6 kJ mol^{-1} associated with **TS-1B** is relatively small. Inspection of the CASSCF natural orbitals and their occupation numbers (see Figure S11 in the Supporting Information) indicates singlet diradical character for **TS-1B**, i.e., a singly occupied oxygen π*- and a pyrrole π-orbital, which form a bonding/antibonding pair. State-specific energy evaluations for the singlet and triplet state at the higher NEVPT2/def-TZVPP level of theory revealed that the singlet/triplet degeneracy is continuously lifted along the structures of the potential energy scan (Figure 3B, lower panel).

The NEVPT2 calculations confirm a negligible activation barrier for C–O bond formation, indicating that dioxygen's entry into the coordination sphere of aluminum (**TS-1A**) is the rate-determining step of the overall reaction.

What is left to elucidate is the critical ISC required for the transformation, which is, however, usually ignored in the discussion of related biotic and abiotic cases. The free superoxide radical anion ($O_2^{\bullet-}$) exhibits strong spin–orbit coupling (SOC) by orbital rotation of the degenerated π*-orbitals.[23,27] This SOC has been proposed as being operative for the ISC in non-iron enzymes such as glucose oxidase or cofactor-free enzymes.[27,28] However, the free superoxide radical anion appears as an unrealistic high-energy state, which seems not accessible in the present case (cf. one-electron redox potential of O_2 and $[^{Me}\mathbf{1}]^-$). Instead, an inner-sphere electron transfer takes place only when $^3O_2$ is coordinating to $[^{Me}\mathbf{1}]^-$. Thus, the superoxide anion is generated not free but directionally bound to aluminum in $^3[^{Me}\mathbf{1}\text{-}O_2]^-$. The degeneracy of the $O_2^{\bullet-}$-located π*-orbitals gets lifted (−7.9 eV vs. 0.9 eV for CASSCF/def2-TZVPP canonical orbitals), and the orbital angular momentum is quenched. Indeed, extremely small absolute spin–orbit coupling matrix elements of less than 0.02 cm^{-1} were computed for $^3[^{Me}\mathbf{1}\text{-}O_2]^-$ (see Chapter S15 of the Supporting Information). Consequently, another ISC mechanism should be operative.[29] With a negligible SOC constant, an ISC is probable if both the energy and the structure of the two spin states are very close (cf. the energy gap law in the weak coupling regime).[29] For the near-degeneracy of the two spin-state energies, the spins need to be decoupled, e.g., by spatial separation. This situation is archetypically found in dihydrogen as a function of the interatomic distance.[30] It is the ligand's redox-activity that enables the desired effect within $^3[^{Me}\mathbf{1}\text{-}O_2]^-$. Upon electron transfer from the calix[4]pyrrolato backbone to dioxygen, the spin density becomes distributed in non-interacting regions of the assembly (Figure 3A), and the energetic degeneracy of both spin states becomes fulfilled. The driving force for the inversion from the triplet to the singlet manifold transpires upon the inclusion of thermal corrections. In contrast to the identical electronic energies of $^3[^{Me}\mathbf{1}\text{-}O_2]^-$ and $^1[^{Me}\mathbf{1}\text{-}O_2]^-$, the Gibbs free energy of the singlet state is computed 21.2 kJ mol^{-1} lower compared to the triplet. This is primarily due to the difference in zero-point vibrational energy (ZPVE), which, under the harmonic approximation, is an outcome of a flatter potential energy surface in the singlet state as compared to the triplet (see the NEVPT2 plot in Figure 3B). Overall, these characteristics point to a spin–vibronic coupling of the two states.[31]

The detailed picture of the reaction between $[^{Me}\mathbf{1}]^-$ and $^3O_2$ allows drawing parallels to processes encountered in dioxygen activating enzymes. For $[^{Me}\mathbf{1}]^-$, the calix[4]pyrrolato ligand is the electron donor in an inner-sphere ligand-to-dioxygen electron transfer, facilitated by the electrophilic activation of $^3O_2$ upon coordination to the redox-inactive, square-planar-coordinated aluminum. For the structurally close iron porphyrins, dioxygen reduction to the superoxide state is found alike, but the electron originates from the Fe^{II} center (Figure 1 C). The ISC in iron-porphyrins is proposed to be mediated by the participation of the open-shell *d*-electrons.[8c] However, $[^{Me}\mathbf{1}]^-$ is a closed-shell molecule lacking any heavy atoms. Hence, the ISC of $[^{Me}\mathbf{1}]^-$ can be projected to metal-free flavoenzymes, such as pyranose 2-oxidase or the oxygenase component of *p*-hydroxyphenylacetate 3-hydroxylase (Figure 1 A), which also comprise only light main-group elements.[5] The aluminum center mimics the histidinium proton side, and the calix[4]pyrrolato ligand takes the role of the flavin cofactor (cf. Figure 1 A).[32] Notably, this analogy suggests that flavoenzymes tackle the ISC by the same principles detailed in the preceding paragraph (weak coupling regime plus spin–vibronic coupling).

The electronic structure of $[^{Me/Et}\mathbf{1}$*-OO$]^-$ was further inspected by spectroscopy and theory. The UV/Vis absorption spectra of $[PPh_4][^{Me}\mathbf{1}$*-OO] or $[PPh_4][^{Et}\mathbf{1}$*-OO] are similar to each other, with broad bands at wavelengths of approximately 340 and 400 nm, reaching deep into the visible region (see Figure S6 in the Supporting Information). Time-dependent density functional calculations on $[^{Me}\mathbf{1}$*-OO$]^-$ identified the respective lowest energy electronic excitations as transitions from the three aromatic pyrrole units to the dearomatized ring. The aromatic pyrroles primarily host the highest occupied molecular orbitals (HOMOs), whereas the dearomatized ring is associated with the lowest unoccupied molecular orbital (LUMO) of $[^{Me}\mathbf{1}$*-OO$]^-$ (Chapter S5 of the Supporting Information). Intriguingly, the ligand-based character of the frontier molecular orbitals of $[^{Me}\mathbf{1}$*-OO$]^-$ contrasts the oxygen atom-centered HOMO/LUMO character found for other peroxides.[33] Common metal alkylperoxides are potent oxidants that may react through several pathways, such as O–O and M–O homolytic cleavage as well as nucleophilic and electrophilic O-atom transfer.[33] In stark contrast, the peroxides $[^{Me/Et}\mathbf{1}$*-OO$]^-$ turned out as remarkably stable. No reactivity was observed toward several nucleophilic and electrophilic substrates, and even the markedly oxophilic triphenylphosphine was left untouched (see Supporting Information for attempted substrates).

However, when storing solutions of $[PPh_4][^{Me/Et}\mathbf{1}$*-OO] in $[D_2]$dichloromethane, a transformation to a new species ($[^{Me/Et}\mathbf{2}]^-$) occurred within 24 hours at room temperature or within 30 minutes at 60 °C (Figure 4 A).

Extensive spectroscopic and quantum chemical investigations provided an excellent foundation for the molecular structure of $[^{Me/Et}\mathbf{2}]^-$ as illustrated in Figure 4 B (in-detail description is given in the Supporting Information in Chapter S10).

In the ESI high-resolution mass spectra of $[^{Me/Et}\mathbf{2}]^-$, peaks were found at *m*/*z* ratios identical to those of $[^{Me/Et}\mathbf{1}$*-OO$]^-$, indicating a rearrangement process without the loss of the OO unit or any other fragment. Evidence for the formation of a C=O-containing functional group was obtained from the emergence of a significant C=O bond stretching band in the IR spectra of $[PPh_4][^{Me/Et}\mathbf{2}]$ (1662 cm^{-1}). The ^1H NMR spectra of $[^{Me/Et}\mathbf{2}]^-$ feature a new set of eight doublet signals in the downfield regime of the spectrum, including one pair with a comparatively large coupling constant of 12.4 Hz (Figure 4 C). A ^{13}C INADEQUATE NMR spectrum of $[^{Et}\mathbf{2}]^-$ unambiguously established the carbon–carbon connectivity, revealing the rupture of the continuous C-atom chain within the calix[4]pyrrolato ligand (Figure 4 D). In the $^1H,^{15}N$ HMBC NMR spectra, ^{15}N resonances at −34.5 ppm ($[^{Me}\mathbf{2}]^-$) and −26.9 ppm ($[^{Et}\mathbf{2}]^-$) were found that differ significantly from the ^{15}N chemical shifts detected for the aromatic pyrrole nitrogen atoms (around −200 ppm) or the dearomatized pyrrole ring in $[^{Me}\mathbf{1}$*-OO$]^-$ (−102.2 ppm). This observation suggests a nitrogen atom with a drastically changed chemical environment, more in the range of imines.[34] Characteristic cross-peaks in the $^1H,^{15}N$ HMBC NMR spectrum of $[^{Me}\mathbf{2}]^-$ with *meso*-methyl groups gave further support for the proposed structure (Figure 4 D).

Lastly, the $^1H,^1H$ NOESY NMR spectrum of $[^{Me}\mathbf{2}]^-$ revealed spatial proximity of the proton β to the carboxylato unit to three methyl groups, whereas none for the α-proton (Figure 4 D). Further, all measured ^1H, ^{13}C, and ^{15}N chemical shifts and the $^3J_{HH}$ spin–spin coupling constants of $[^{Me}\mathbf{2}]^-$ were compared with GIAO-DFT-computed values (PBE0/IGLO-II). Ideal matching was achieved for $[^{Me}\mathbf{2}]^-$, thus further validating the correct structure assignment (Figure 4 E). Hence, the alkylperoxido motive in $[^{Me/Et}\mathbf{1}$*-OO$]^-$ rearranges to an α,β-unsaturated carboxylato grouping in $[^{Me/Et}\mathbf{2}]^-$, concomitant with the oxidative α-cleavage of the dearomatized pyrrole ring. The aluminum center is released from its square pyramidal coordination environment in $[^{Me/Et}\mathbf{1}$*-OO$]^-$ and resides within a slightly distorted tetrahedron spanned by the three aromatic pyrrolato moieties and the carboxylato group. The DFT structure optimization showed that the imine nitrogen is non-coordinating. It also supports the *E*-configuration of the imine functional group. The *Z*-configuration cannot reflect the experimentally observed spatial arrangement and is also energetically less favorable (26.1 kJ mol^{-1}) than the *E*-stereoisomer. The calculated Gibbs free reaction enthalpy for the reaction from $[^{Me}\mathbf{1}$*-OO$]^-$ to $[^{Me}\mathbf{2}]^-$ of −280.3 kJ mol^{-1} confirms the thermodynamic driving force of the transformation.

To the best of our knowledge, a direct oxidative α-cleavage of a pyrrole ring is unprecedented in the literature. Overall, the reaction sequence from $[^{Me}\mathbf{1}]^-$ to $[^{Me}\mathbf{2}]^-$ describes the incorporation of two oxygen atoms stemming from O_2 into an aromatic ring system.

To explain this transformation, quantum chemical calculations were conducted (Figure 5). The initial step is the heterolytic breaking of the exocyclic C–C bond α to the alkylperoxido moiety (**TS-2A**).[35] This leads to the dearomatization of the adjacent pyrrole ring and the rearomatization of the peroxo-containing ring in the resulting intermediate (**Int-2A**). This step is energetically favored over the O–O bond cleavage in $[^{Me}\mathbf{1}$*-OO$]^-$ that would lead to $[^{Me}\mathbf{1}$*-O | O$]^-$ (Figure 5, left path). From **Int-2A**, the reaction proceeds by

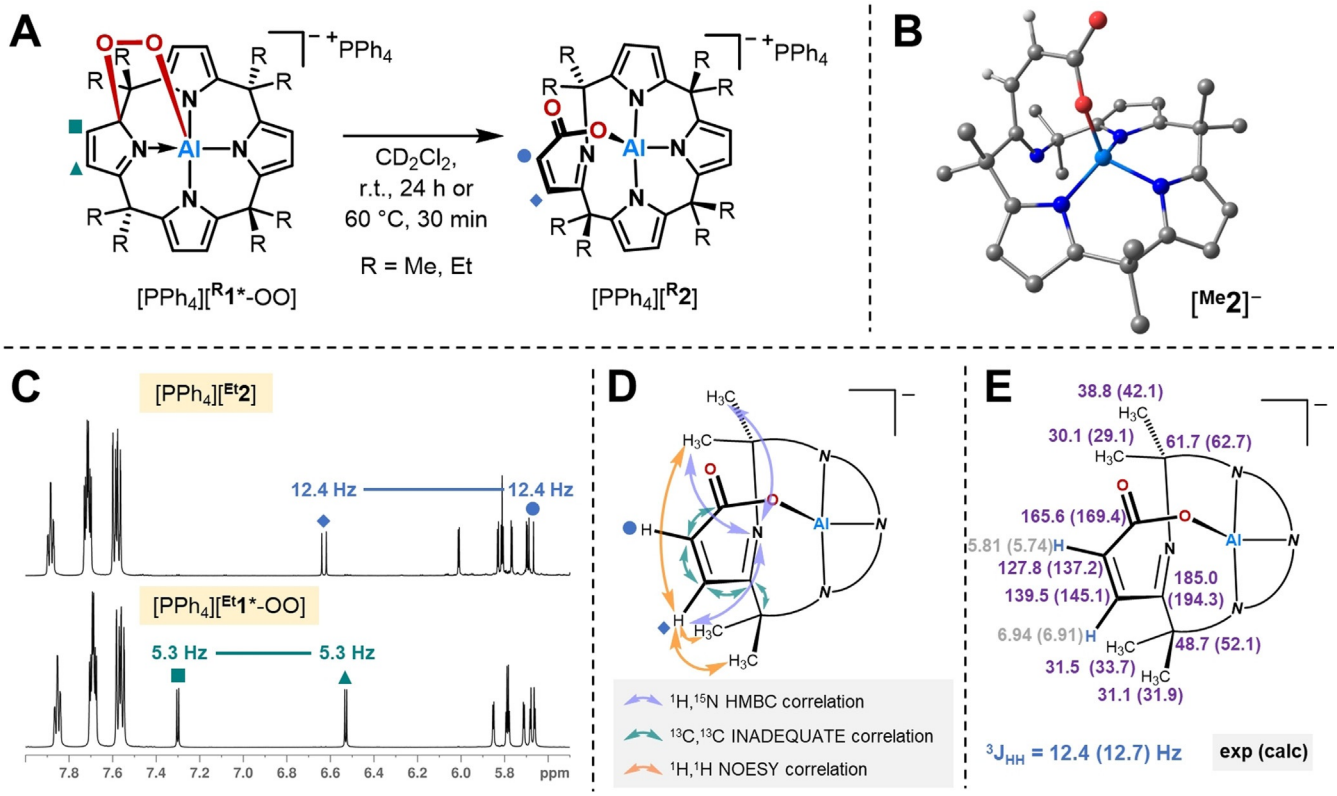

Figure 4. A) Reaction scheme for the transformation of the alkylperoxido aluminates, [PPh_4][$^{Me/Et}$**1***-OO], to the carboxylato aluminates, [PPh_4]-[$^{Me/Et}$**2**]. B) Molecular structure of [^{Me}**2**]$^-$ optimized at the B97M-D3(BJ)/def2-TZVPP level of theory. All hydrogen atoms except for the two attached to the C–C double bond α to the carboxylato group were omitted for clarity. C) Tetraphenylphosphonium/pyrrole section of the ^{1}H NMR spectrum (600 MHz, CD_2Cl_2) of [PPh_4][^{Et}**1***-OO] and [PPh_4][^{Et}**2**]. D) ^{1}H,^{15}N HMBC, ^{13}C INADEQUATE, and ^{1}H,^{1}H NOESY NMR correlations observed for [PPh_4][$^{Me/Et}$**2**]. The INADEQUATE NMR spectrum was measured for [PPh_4][^{Et}**2**]. E) Chemical shifts (given in ppm) and the characteristic $^3J_{HH}$ spin–spin coupling constant of [^{Me}**2**]$^-$ determined by experiment and calculation on the PBE0/IGLO-II level of theory.

splitting the O–O bond via a transition state (**TS-2B**), most likely exhibiting open-shell singlet character. Interestingly, in **TS-2B**, the dearomatized pyrrole ring is detached from the aluminum center, which renders the hemilability of the ligand beneficial for the cleavage of the O–O bond. In the subsequent step, the ester moiety is formed by C–O bond formation and C–N bond cleavage, resulting in **Int-2C**. This last intermediate converts to the final product [^{Me}**2**]$^-$ by nucleophilic attack of the imine group on the C–C double bond and the reattachment of the rearomatized pyrrole ring to the aluminum atom (**TS-2D**). The entire reaction path from **TS-2B** to **Int-2C** was verified by following the intrinsic reaction coordinate (IRC) on the closed-shell potential energy surface starting from **TS-2B**. Computing the open-shell singlet energy for selected IRC structures with the broken-symmetry approach discloses the open-shell singlet states along the path as even more favorable (see Chapter S13 of the Supporting Information for a full discussion).

In total, this analysis demonstrates that aromatization/dearomatization and ligand hemilability are key for provoking a weakening of the O–O bond that makes this process feasible at room temperature. Both features are prevalent in d-block metal coordination chemistry but less evident for p-block compounds.[36]

Conclusion

Calix[4]pyrrolato aluminates ([$^{Me/Et}$**1**]$^-$) react spontaneously with molecular oxygen to afford alkylperoxido aluminates ([$^{Me/Et}$**1***-OO]$^-$). During the initial stage of the reaction, O_2 coordinates end-on to [$^{Me/Et}$**1**]$^-$. This binding is facilitated by the structural constraint-induced Lewis acidity in the square-planar aluminum anion. An inner-sphere electron transfer from the redox-active ligand to dioxygen leads into the weak coupling regime. Here, the ISC becomes possible due to both spin states' near-energetic degeneracy at identical structures—despite the absence of heavy elements and negligible computed spin–orbit coupling matrix elements—potentially facilitated by spin–vibronic coupling. Ligand aromatization/dearomatization steps and ligand hemilability lead to a subsequent oxidative α-cleavage of a pyrrole unit and finalize the overall incorporation of two oxygen atoms from air into the aromatic ring.

Metal–ligand or cofactor–protein cooperativity has been long recognized as a central tool of enzymatic function.[36–37] However, its role during dioxygen activation and metabolism is less well understood. The calix[4]pyrrolato aluminates are model systems that allow connections with important dioxygen-related enzymes.

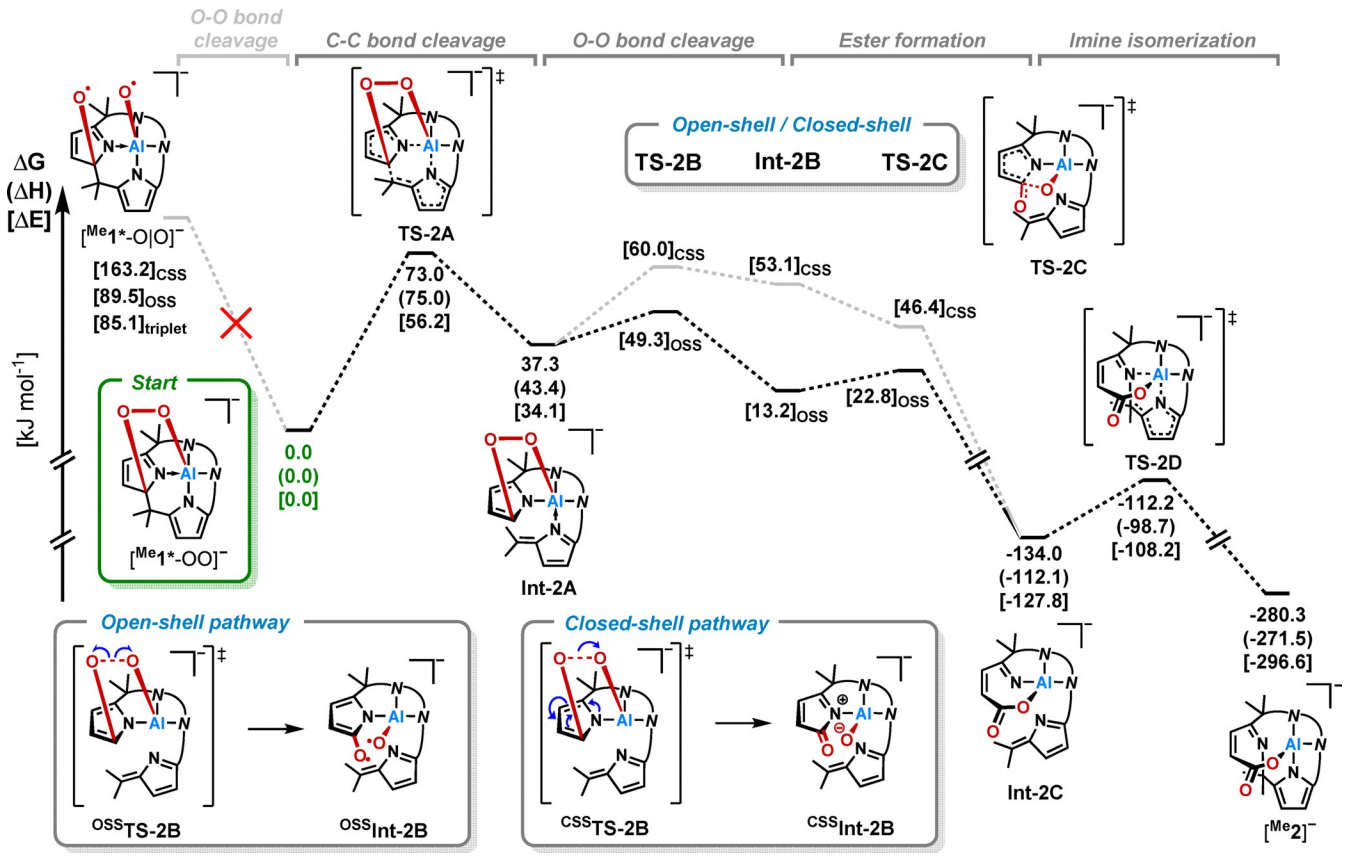

Figure 5. Proposed mechanistic pathway and calculated energy profile for the transformation from $[^{Me}\mathbf{1}^{*}\text{-OO}]^{-}$ to $[^{Me}\mathbf{2}]^{-}$ (B97M-D3(BJ)/def2-TZVPP). The given Gibbs free energies and enthalpies include COSMO-RS(CH_2Cl_2) solvation correction. Open-shell singlet (OSS) energies were estimated employing the broken-symmetry ansatz and Yamaguchi's equation for approximate spin projection on the closed-shell singlet (CSS) structures (see the Supporting Information for further details).

1) Most obviously, the porphyrinogenic $[^{Me/Et}\mathbf{1}]^{-}$ has a structural relationship with iron porphyrins (Figure 1C). Although both complexes share a metal-centered dioxygen attachment, they differ in the ligand-centered redox (in)-activity and the ultimate binding mode.

2) The MLC-dioxygen binding mode in $[^{Me/Et}\mathbf{1}^{*}\text{-OO}]^{-}$ is analogous to non-heme extra- or intradiol dioxygenases (Figure 1B). However, since the open-shell iron center is missing in $[^{Me/Et}\mathbf{1}]^{-}$, the actual spin barrier is bypassed by another mechanism. Indeed, a connection is found with flavin-dependent enzymes (Figure 1A). The aluminum Lewis acidic center mimics the side chain histidinium proton of flavoenzymes that becomes operative during PCET, and the redox-active calix[4]pyrrolato ligand serves as the electron donor (flavin equivalent). The detailed insights into the ISC mechanism obtained for $[^{Me/Et}\mathbf{1}]^{-}$ in the present study can be projected to metal- or cofactor-free enzymes and offer new insights for spin-forbidden processes in aerobic life.

From a biochemical perspective, the herewith presented findings substantiate the importance of constraint and cooperativity in dioxygen metabolism. From a synthetic view, this study expands structural constraints for dioxygen activation. Ultimately, it offers a starting point to exploit air's inherent redox potential with earth-abundant elements beyond iron or other transition metals.

Acknowledgements

We thank Prof. H.-J. Himmel for his constant support. Financial support was provided through an ERC starting grant (pCx4All, L.G.). L.M.S. is grateful to the Studienstiftung des deutschen Volkes for support. C.E. and G.G. gratefully acknowledge the Klaus Tschira Foundation for financial and administrative support. For computational resources, we acknowledge the state of Baden-Württemberg through bwHPC (JUSTUS 2), the Interdisciplinary Center for Scientific Computing (IWR) of Heidelberg University, and the Heidelberg Institute for Theoretical Studies (HITS gGmbH). Dr. F. Ebner is acknowledged for providing cyclic voltammetry data and E. Filbeck for carrying out the SCXRD measurement. Open access funding enabled and organized by Projekt DEAL.

Conflict of interest

The authors declare no conflict of interest.

Keywords: aluminum · dioxygen activation · intersystem crossing · metal–ligand cooperativity · structural constraint

[1] a) B. G. Malmstrom, *Annu. Rev. Biochem.* **1982**, *51*, 21 – 59; b) B. A. Palfey, D. P. Ballou, V. Massey, in *Active Oxygen in Biochemistry* (Eds.: J. S. Valentine, C. S. Foote, A. Greenberg, J. F. Liebman), Springer Netherlands, Dordrecht, **1995**, pp. 37 – 83; c) T. D. H. Bugg, *Curr. Opin. Chem. Biol.* **2001**, *5*, 550 – 555; d) A. Decker, E. I. Solomon, *Curr. Opin. Chem. Biol.* **2005**, *9*, 152 – 163.

[2] E. Romero, J. R. Gómez Castellanos, G. Gadda, M. W. Fraaije, A. Mattevi, *Chem. Rev.* **2018**, *118*, 1742 – 1769.

[3] a) E. G. Kovaleva, J. D. Lipscomb, *Nat. Chem. Biol.* **2008**, *4*, 186 – 193; b) M. Costas, M. P. Mehn, M. P. Jensen, L. Que, *Chem. Rev.* **2004**, *104*, 939 – 986.

[4] a) X. Huang, J. T. Groves, *Chem. Rev.* **2018**, *118*, 2491 – 2553; b) M. Wikström, K. Krab, V. Sharma, *Chem. Rev.* **2018**, *118*, 2469 – 2490.

[5] a) T. Wongnate, P. Surawatanawong, S. Visitsatthawong, J. Sucharitakul, N. S. Scrutton, P. Chaiyen, *J. Am. Chem. Soc.* **2014**, *136*, 241 – 253; b) S. Visitsatthawong, P. Chenprakhon, P. Chaiyen, P. Surawatanawong, *J. Am. Chem. Soc.* **2015**, *137*, 9363 – 9374.

[6] a) J. Rosenthal, D. G. Nocera, *Acc. Chem. Res.* **2007**, *40*, 543 – 553; b) V. R. I. Kaila, M. I. Verkhovsky, M. Wikström, *Chem. Rev.* **2010**, *110*, 7062 – 7081.

[7] B. F. Minaev, H. Ågren, V. O. Minaeva, in *Handbook of Computational Chemistry* (Eds.: J. Leszczynski, A. Kaczmarek-Kedziera, T. Puzyn, M. G. Papadopoulos, H. Reis, M. K. Shukla), Springer International Publishing, Cham, **2017**, pp. 1557 – 1587.

[8] a) K. P. Jensen, U. Ryde, *J. Biol. Chem.* **2004**, *279*, 14561 – 14569; b) P. E. M. Siegbahn, T. Borowski, *Acc. Chem. Res.* **2006**, *39*, 729 – 738; c) M. Y. M. Pau, J. D. Lipscomb, E. I. Solomon, *Proc. Natl. Acad. Sci. USA* **2007**, *104*, 18355 – 18362; d) J. Ribas-Ariño, J. J. Novoa, *Chem. Commun.* **2007**, 3160 – 3162; e) A. Hernández-Ortega, M. G. Quesne, S. Bui, D. J. Heyes, R. A. Steiner, N. S. Scrutton, S. P. de Visser, *J. Am. Chem. Soc.* **2015**, *137*, 7474 – 7487; f) Y. Kitagawa, Y. Chen, N. Nakatani, A. Nakayama, J. Hasegawa, *Phys. Chem. Chem. Phys.* **2016**, *18*, 18137 – 18144; g) Y. Luo, Y.-J. Liu, *J. Phys. Chem. A* **2019**, *123*, 4354 – 4359; h) K. Saito, Y. Watabe, T. Fujihara, T. Takayanagi, J.-y. Hasegawa, *J. Comput. Chem.* **2020**, *41*, 1130 – 1138; i) K. Saito, Y. Watabe, T. Miyazaki, T. Takayanagi, J.-y. Hasegawa, *J. Comput. Chem.* **2020**, *41*, 2527 – 2537.

[9] M. R. A. Blomberg, T. Borowski, F. Himo, R.-Z. Liao, P. E. M. Siegbahn, *Chem. Rev.* **2014**, *114*, 3601 – 3658.

[10] a) P. E. M. Siegbahn, F. Haeffner, *J. Am. Chem. Soc.* **2004**, *126*, 8919 – 8932; b) T. Borowski, P. E. M. Siegbahn, *J. Am. Chem. Soc.* **2006**, *128*, 12941 – 12953; c) E. G. Kovaleva, J. D. Lipscomb, *Science* **2007**, *316*, 453; d) M. Y. M. Pau, M. I. Davis, A. M. Orville, J. D. Lipscomb, E. I. Solomon, *J. Am. Chem. Soc.* **2007**, *129*, 1944 – 1958; e) P. Kumar, S. V. Lindeman, A. T. Fiedler, *J. Am. Chem. Soc.* **2019**, *141*, 10984 – 10987.

[11] a) P. A. Gale, J. L. Sessler, V. Král, *Chem. Commun.* **1998**, 1 – 8; b) K. M. Kadish, K. M. Smith, R. Guilard, *The porphyrin handbook. Vol. 3*, Academic Press, San Diego, London, **2000**; c) C. Floriani, *Chem. Commun.* **1996**, 1257 – 1263; d) A. Baeyer, *Ber. Dtsch. Chem. Ges.* **1886**, *19*, 2184 – 2185.

[12] a) J.-M. Benech, L. Bonomo, E. Solari, R. Scopelliti, C. Floriani, *Angew. Chem. Int. Ed.* **1999**, *38*, 1957 – 1959; *Angew. Chem.* **1999**, *111*, 2107 – 2109; b) L. Bonomo, E. Solari, R. Scopelliti, C. Floriani, N. Re, *J. Am. Chem. Soc.* **2000**, *122*, 5312 – 5326; c) M. Harmjanz, H. S. Gill, M. J. Scott, *J. Am. Chem. Soc.* **2000**, *122*, 10476 – 10477; d) J. Bachmann, D. G. Nocera, *J. Am. Chem. Soc.* **2004**, *126*, 2829 – 2837; e) J. Bachmann, D. G. Nocera, *J. Am. Chem. Soc.* **2005**, *127*, 4730 – 4743.

[13] F. Ebner, H. Wadepohl, L. Greb, *J. Am. Chem. Soc.* **2019**, *141*, 18009 – 18012.

[14] a) L. Greb, F. Ebner, Y. Ginzburg, L. M. Sigmund, *Eur. J. Inorg. Chem.* **2020**, 3030 – 3047; b) F. Ebner, L. M. Sigmund, L. Greb, *Angew. Chem. Int. Ed.* **2020**, *59*, 17118 – 17124; *Angew. Chem.* **2020**, *132*, 17266 – 17272; c) L. M. Sigmund, L. Greb, *Chem. Sci.* **2020**, *11*, 9611 – 9616; d) F. Ebner, P. Mainik, L. Greb, *Chem. Eur. J.* **2021**, *27*, 5120 – 5124.

[15] M. C. Weiss, V. L. Goedken, *J. Am. Chem. Soc.* **1976**, *98*, 3389 – 3392.

[16] S. Dutta, S.-M. Peng, S. Bhattacharya, *Inorg. Chem.* **2000**, *39*, 2231 – 2234.

[17] a) P. Barbaro, C. Bianchini, C. Mealli, A. Meli, *J. Am. Chem. Soc.* **1991**, *113*, 3181 – 3183; b) J. R. Bleeke, Y. F. Xie, L. Bass, M. Y. Chiang, *J. Am. Chem. Soc.* **1991**, *113*, 4703 – 4704.

[18] a) P. Holze, T. Corona, N. Frank, B. Braun-Cula, C. Herwig, A. Company, C. Limberg, *Angew. Chem. Int. Ed.* **2017**, *56*, 2307 – 2311; *Angew. Chem.* **2017**, *129*, 2347 – 2351; b) C. A. Rettenmeier, H. Wadepohl, L. H. Gade, *Angew. Chem. Int. Ed.* **2015**, *54*, 4880 – 4884; *Angew. Chem.* **2015**, *127*, 4962 – 4966.

[19] a) M. L. Scheuermann, U. Fekl, W. Kaminsky, K. I. Goldberg, *Organometallics* **2010**, *29*, 4749 – 4751; b) M. L. Scheuermann, A. T. Luedtke, S. K. Hanson, U. Fekl, W. Kaminsky, K. I. Goldberg, *Organometallics* **2013**, *32*, 4752 – 4758; c) M. L. Scheuermann, K. I. Goldberg, *Chem. Eur. J.* **2014**, *20*, 14556 – 14568.

[20] a) G. A. Abakumov, A. I. Poddel'sky, E. V. Grunova, V. K. Cherkasov, G. K. Fukin, Y. A. Kurskii, L. G. Abakumova, *Angew. Chem. Int. Ed.* **2005**, *44*, 2767 – 2771; *Angew. Chem.* **2005**, *117*, 2827 – 2831; b) V. K. Cherkasov, G. A. Abakumov, E. V. Grunova, A. I. Poddel'sky, G. K. Fukin, E. V. Baranov, Y. V. Kurskii, L. G. Abakumova, *Chem. Eur. J.* **2006**, *12*, 3916 – 3927; c) G. K. Fukin, E. V. Baranov, A. I. Poddel′sky, V. K. Cherkasov, G. A. Abakumov, *ChemPhysChem* **2012**, *13*, 3773 – 3776; d) M. V. Arsenyev, M. P. Shurygina, A. I. Poddel'sky, N. O. Druzhkov, S. A. Chesnokov, G. K. Fukin, V. K. Cherkasov, G. A. Abakumov, *J. Polym. Res.* **2013**, *20*, 98; e) S. A. Chesnokov, N. A. Lenshina, M. V. Arsenyev, R. S. Kovylin, M. A. Baten′kin, A. I. Poddel′sky, G. A. Abakumov, *Appl. Organomet. Chem.* **2017**, *31*, e3553.

[21] a) W. M. Cleaver, A. R. Barron, *J. Am. Chem. Soc.* **1989**, *111*, 8966 – 8967; b) A. R. Barron, *Chem. Soc. Rev.* **1993**, *22*, 93 – 99; c) J. Lewiński, J. Zachara, E. Grabska, *J. Am. Chem. Soc.* **1996**, *118*, 6794 – 6795; d) T. K. Wood, W. E. Piers, B. A. Keay, M. Parvez, *Angew. Chem. Int. Ed.* **2009**, *48*, 4009 – 4012; *Angew. Chem.* **2009**, *121*, 4069 – 4072; e) L. Kong, W. Lu, Y. Li, R. Ganguly, R. Kinjo, *Angew. Chem. Int. Ed.* **2016**, *55*, 14718 – 14722; *Angew. Chem.* **2016**, *128*, 14938 – 14942; f) T. Wang, G. Kehr, L. Liu, S. Grimme, C. G. Daniliuc, G. Erker, *J. Am. Chem. Soc.* **2016**, *138*, 4302 – 4305; g) J. W. Taylor, A. McSkimming, C. F. Guzman, W. H. Harman, *J. Am. Chem. Soc.* **2017**, *139*, 11032 – 11035; h) J. Lewiński, J. Zachara, P. Goś, E. Grabska, T. Kopeć, I. Madura, W. Marciniak, I. Prowotorow, *Chem. Eur. J.* **2000**, *6*, 3215 – 3227; i) H. Zhu, J. Chai, V. Jancik, H. W. Roesky, W. A. Merrill, P. P. Power, *J. Am. Chem. Soc.* **2005**, *127*, 10170 – 10171; j) W. Uhl, B. Jana, *Chem. Eur. J.* **2008**, *14*, 3067 – 3071; k) E. Tsurumaki, J. Sung, D. Kim, A. Osuka, *Angew. Chem. Int. Ed.* **2016**, *55*, 2596 – 2599; *Angew. Chem.* **2016**, *128*, 2642 – 2645; l) A. C. Stelzer, P. Hrobárik, T. Braun, M. Kaupp, B. Braun-Cula, *Inorg. Chem.* **2016**, *55*, 4915 – 4923; m) B. Jana, C. Honaker, W. Uhl, *J. Organomet. Chem.* **2018**, *856*, 78 – 86; n) B. Wang, R. Kinjo, *Chem. Sci.* **2019**, *10*, 2088 – 2092; o) A. Rola-Noworyta, T. Pietrzak, V. Szejko, I. Justyniak, J. Lewiński, *Inorg. Chem.* **2020**, *59*, 13807 – 13811.

[22] S. S. Kumar, S. Singh, H. W. Roesky, J. Magull, *Inorg. Chem.* **2005**, *44*, 1199 – 1201.

[23] K. Huber, G. Herzberg, *Molecular spectra and molecular structure : iv. constants of diatomic molecules*, Springer, New York, **2013**.

[24] J. Jubb, C. Floriani, A. Chiesi-Villa, C. Rizzoli, *J. Am. Chem. Soc.* **1992**, *114*, 6571 – 6573.
[25] P. S. Singh, D. H. Evans, *J. Phys. Chem. B* **2006**, *110*, 637 – 644.
[26] W. T. Borden, R. Hoffmann, T. Stuyver, B. Chen, *J. Am. Chem. Soc.* **2017**, *139*, 9010 – 9018.
[27] R. Prabhakar, P. E. M. Siegbahn, B. F. Minaev, H. Ågren, *J. Phys. Chem. B* **2002**, *106*, 3742 – 3750.
[28] B. F. Minaev, *Chem. Phys.* **2019**, *521*, 61 – 68.
[29] a) C. M. Marian, *Wiley Interdiscip. Rev.: Comput. Mol. Sci.* **2012**, *2*, 187 – 203; b) C. M. Marian, *Annu. Rev. Phys. Chem.* **2021**, *72*, 617 – 640.
[30] in *Quantum Theory of Magnetism: Magnetic Properties of Materials* (Ed.: R. M. White), Springer, Berlin, Heidelberg, **2007**, pp. 33 – 83.
[31] T. J. Penfold, E. Gindensperger, C. Daniel, C. M. Marian, *Chem. Rev.* **2018**, *118*, 6975 – 7025.
[32] S. Fukuzumi, K. Ohkubo, Y.-M. Lee, W. Nam, *Chem. Eur. J.* **2015**, *21*, 17548 – 17559.
[33] a) G. Sosnovsky, J. H. Brown, *Chem. Rev.* **1966**, *66*, 529 – 566; b) P. B. Brindley, in *Peroxides (1983)*, **1983**, pp. 807 – 828, PATAI'S Chemistry of Functional Groups, John-Wiley & Sons, Chichester; c) W. Adam, F. Deutsche, *Peroxide chemistry : mechanistic and preparative aspects of oxygen transfer : research report*, Wiley-VCH, Weinheim, **2000**; d) B. Meunier, *Metal-Oxo and Metal-Peroxo Species in Catalytic Oxidations*, Springer, Berlin, **2013**.
[34] G. J. Martin, M. L. Martin, J.-P. Gouesnard, *^{15}N-NMR Spectroscopy*, Springer, Berlin, Heidelberg, **1981**.
[35] G. Solari, E. Solari, G. Lemercier, C. Floriani, A. Chiesi-Villa, C. Rizzoli, *Inorg. Chem.* **1997**, *36*, 2691 – 2695.
[36] J. R. Khusnutdinova, D. Milstein, *Angew. Chem. Int. Ed.* **2015**, *54*, 12236 – 12273; *Angew. Chem.* **2015**, *127*, 12406 – 12445.
[37] M. D. Wodrich, X. Hu, *Nat. Rev. Chem.* **2018**, *2*, 0099.
[38] Deposition Number 2072557 ([^{Me}**1***-OO]$^-$) contains the supplementary crystallographic data for this paper. These data are provided free of charge by the joint Cambridge Crystallographic Data Centre and Fachinformationszentrum Karlsruhe Access Structures service www.ccdc.cam.ac.uk/structures.

Manuscript received: April 14, 2021
Accepted manuscript online: May 6, 2021
Version of record online: June 8, 2021

